

Ghost imaging with intense fields from chaotically-seeded parametric downconversion

Emiliano Puddu and Alessandra Andreoni

Dipartimento di Fisica e Matematica, Università degli Studi dell'Insubria, Istituto Nazionale per la Fisica della Materia (C.N.R.-I.N.F.M.), Como, Italy

Ivo Pietro Degiovanni

Istituto Nazionale di Ricerca Metrologica, Torino, Italy

Maria Bondani

National Laboratory for Ultrafast and Ultraintense Optical Science, C.N.R.-I.N.F.M., Como, Italy

Stefania Castelletto

Physics School, Melbourne University, Victoria, Australia

We present the first experimental demonstration of ghost imaging realized with intense beams generated by a parametric downconversion interaction seeded with pseudo-thermal light. As expected, the real image of the object is reconstructed satisfying the thin-lens equation. We show that the experimental visibility of the reconstructed image is in accordance with the theoretically expected one. © 2019 Optical Society of America

OCIS codes: 270.0270, 190.2620, 270.5290, 030.0030, 100.0100

Ghost imaging capability was initially attributed only to entangled photon pairs,¹ but in more recent works it has been ascertained also for classically correlated fields, both in the single photon regime^{2,3} and in the continuous variable regime.⁴ The main result of all these schemes is the non-local imaging of objects both in near- and far-field.⁵ A general ghost-imaging scheme involves a source of correlated bipartite field and two propagation arms usually called Test and Reference. In the Test arm the object to be imaged is inserted and a bucket (or a pointlike) detector measures the light transmitted by the object. The Reference arm contains an optical setup suitable for reconstructing the image of the object (or its Fourier transform) and a position-sensitive detector.

In this Letter we show a ghost imaging experiment performed by using the intense fields generated by parametric downconversion (PDC) seeded with multimode chaotic light. As usual in ghost imaging experiments, the technique adopted for the retrieval of the image consists of the measurement and the evaluation of the fourth-order correlation between the fields at the detection planes.

In Fig. 1 we show our experimental setup. We injected a coherent collimated pump beam

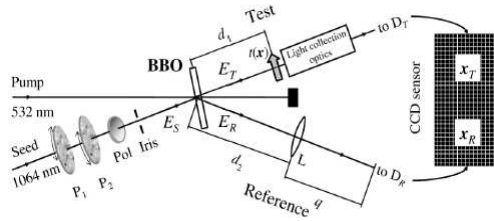


Fig. 1. Experimental setup: $P_{1,2}$, independently rotating ground glass plates; Pol, polarizer; $t(\mathbf{x})$, object transmission function; L, lens. The CCD sensor is used to detect both Test and Reference beams.

($\lambda = 532$ nm) and a seed beam ($\lambda = 1064$ nm) into a crystal of β -BaB₂O₄ (BBO, cut angle 22.8 deg, 10 mm×10 mm×3 mm, Fujian Castech Crystals, China). Both pump and seed beams were provided by an amplified Q-switched Nd:YAG laser (GCR-4, 10 Hz repetition rate, 7 ns pulse duration of the fundamental pulse, Spectra-Physics, USA). The seed field was randomized by passing it through two independently rotating ground glass plates,⁶ P_1 and P_2 in order to obtain a pseudo-thermal statistics. The speckles on the object plane resulted to be about 320 μ m in diameter as evaluated by spatial autocorrelation. The object was a hole of 1.6 mm diameter crossed by a straight wire of 0.5 mm caliber. As the D_T and D_R detectors, we used a single CCD camera (CA-D1-256T, 16 μ m×16 μ m pixel area, 12 bit resolution, Dalsa, Canada). The CCD sensor, also depicted in Fig. 1, for one half recorded the single-shot intensity Maps in the Reference arm, $\mathcal{I}_R(\mathbf{x}_R)$, and for the other half realized the bucket detector of the Test arm. In the following, \mathcal{I}_T designates the sum of the contents of 110 × 110 pixels of D_T in a single shot. The Test arm includes free propagation over distance $d_1 = 60$ cm from BBO to object, transmission function $t(\mathbf{x})$, and light collection optics in front of D_T . The Reference arm contains free propagation from BBO to lens L (focal length

$f = 400$ mm, $d_2 = 60$ cm) and from L to the CCD camera (distance $q = 60$ cm). Distances d_1 , d_2 and q must satisfy $1/(d_1 + d_2) + 1/q = 1/f$ to give an imaging system with magnification factor $M = q/(d_1 + d_2)$.¹ In our case $M = 0.5$. We describe the PDC interaction by using the input-output relations⁷

$$b_i(\mathbf{q}) = U_i(\mathbf{q})a_i(\mathbf{q}) + V_i(\mathbf{q})a_j^\dagger(-\mathbf{q}) \quad i = R, T; \quad i \neq j. \quad (1)$$

that link the output operators $b_i(\mathbf{q})$ to the input operators $a_i(\mathbf{q})$, where $|U_i(\mathbf{q})|^2 - |V_i(\mathbf{q})|^2 = 1$. We take $a_R(\mathbf{q})$ in the vacuum state and $a_T(\mathbf{q})$ in the multimode thermal state represented by the density matrix

$$\rho_T = \prod_{\mathbf{q}}^{\otimes} \left\{ \sum_{m=0}^{\infty} p_T(m(\mathbf{q})) |m(\mathbf{q})\rangle_{TT} \langle m(\mathbf{q})| \right\}, \quad (2)$$

where $|m(\mathbf{q})\rangle$ denotes the Fock state with m photons in mode \mathbf{q} and $p_T(m) = [n_{th}(\mathbf{q})]^m / [1 + n_{th}(\mathbf{q})]^{m+1}$ is the photon number distribution on the single mode for $n_{th}(\mathbf{q})$ mean photon number. The density matrix at the output is then⁸

$$\begin{aligned} \rho_{out} = & \prod_{\mathbf{q}}^{\otimes} \sum_{n(\mathbf{q})} p_T[n(\mathbf{q})] \sum_{n_1(\mathbf{q}), n_2(\mathbf{q})} F[n(\mathbf{q}), n_1(\mathbf{q}), n_2(\mathbf{q})] \\ & |n(\mathbf{q}) + n_1(\mathbf{q})\rangle_{TT} \langle n(\mathbf{q}) + n_2(\mathbf{q})| \otimes |n_1(-\mathbf{q})\rangle_{RR} \langle n_2(-\mathbf{q})| \end{aligned} \quad (3)$$

where we have defined

$$\begin{aligned} F[n(\mathbf{q}), n_1(\mathbf{q}), n_2(\mathbf{q})] = & \frac{[n_{\text{PDC}}(\mathbf{q})]^{\frac{n_1(\mathbf{q})+n_2(\mathbf{q})}{2}}}{[1 + n_{\text{PDC}}(\mathbf{q})]^{n(\mathbf{q})+1+\frac{n_1(\mathbf{q})+n_2(\mathbf{q})}{2}}} \\ & \times \sqrt{\frac{[n(\mathbf{q}) + n_1(\mathbf{q})]!}{n(\mathbf{q})!n_1(\mathbf{q})!}} \sqrt{\frac{[n(\mathbf{q}) + n_2(\mathbf{q})]!}{n(\mathbf{q})!n_2(\mathbf{q})!}} \end{aligned} \quad (4)$$

being $n_{\text{PDC}}(\mathbf{q}) = |V_R(\mathbf{q})|^2$ the mean photon number per mode generated by spontaneous PDC. By direct application of the Peres-Horodecki-Simon criterion⁹⁻¹¹ it can be demonstrated that the state ρ_{out} is inseparable for any value of $n_{th}(\mathbf{q})$.⁸

The reconstruction of the image is achieved by the computation of the correlation function, $G^{(2)}(\mathbf{x}_R)$. This procedure is equivalent first to evaluate the correlation function between $I_R(\mathbf{x}_R)$ and $I_T(\mathbf{x}_T)$

$$\mathcal{G}^{(2)}(\mathbf{x}_R, \mathbf{x}_T) = \langle I_R(\mathbf{x}_R)I_T(\mathbf{x}_T) \rangle - \langle I_R(\mathbf{x}_R) \rangle \langle I_T(\mathbf{x}_T) \rangle, \quad (5)$$

where $\langle I_i(\mathbf{x}_i) \rangle = \langle c_i^\dagger(\mathbf{x}_i)c_i(\mathbf{x}_i) \rangle$ ($i = R, T$) is the mean intensity of the i -th beam and $\langle I_R(\mathbf{x}_R)I_T(\mathbf{x}_T) \rangle = \langle c_R^\dagger(\mathbf{x}_R)c_R(\mathbf{x}_R)c_T^\dagger(\mathbf{x}_T)c_T(\mathbf{x}_T) \rangle$, and then to perform the integration

$$G^{(2)}(\mathbf{x}_R) = \int d\mathbf{x}_T \mathcal{G}^{(2)}(\mathbf{x}_R, \mathbf{x}_T). \quad (6)$$

By representing the propagation to D_T and D_R by the corresponding impulse response functions $h_R(\mathbf{x}_R, \mathbf{x}'_R)$ and $h_T(\mathbf{x}_T, \mathbf{x}'_T)$, whose derivation is straightforward,¹² the field operators at the detection planes become $c_i(\mathbf{x}_i) = \int d\mathbf{x}'_i h_i(\mathbf{x}_i, \mathbf{x}'_i) b_i(\mathbf{x}'_i)$, where $b_i(\mathbf{x}) = \int d\mathbf{q}/(2\pi) \exp(i\mathbf{q} \cdot \mathbf{x}) b_i(\mathbf{q})$. By means of Eq.s (1) we can demonstrate⁸ that the factorization rule for $\langle b_R^\dagger(\mathbf{x}''_R) b_R(\mathbf{x}'_R) b_T^\dagger(\mathbf{x}''_T) b_T(\mathbf{x}'_T) \rangle$ is the same as that for spontaneous PDC.⁷ Thus in the degenerate case Eq. (5) becomes

$$\mathcal{G}^{(2)}(\mathbf{x}_R, \mathbf{x}_T) = \left| \int d\mathbf{x}'_R \int d\mathbf{x}'_T h_R(\mathbf{x}_R, \mathbf{x}'_R) h_T(\mathbf{x}_T, \mathbf{x}'_T) \langle b_R(\mathbf{x}'_R) b_T(\mathbf{x}'_T) \rangle \right|^2, \quad (7)$$

which leads to

$$G^{(2)}(\mathbf{x}_R) \propto |t(-M\mathbf{x}_R)|^2 \int d\mathbf{x}_T n_{\text{PDC}} \left(\frac{-2\pi\mathbf{x}_T}{\lambda f} \right) \times \left[1 + n_{\text{PDC}} \left(\frac{+2\pi\mathbf{x}_T}{\lambda f} \right) \right] \left[1 + n_{th} \left(\frac{-2\pi\mathbf{x}_T}{\lambda f} \right) \right]^2. \quad (8)$$

In our experiment we estimate $n_{\text{PDC}} \simeq 0.5$ and $n_{th} \simeq 10^{12}$ per spatial mode. As expected the correlation function in Eq. (8) reproduces the object transmission function and depends on the properties of our source through the mean photon numbers of downconverted fields and of the chaotic seeding field.

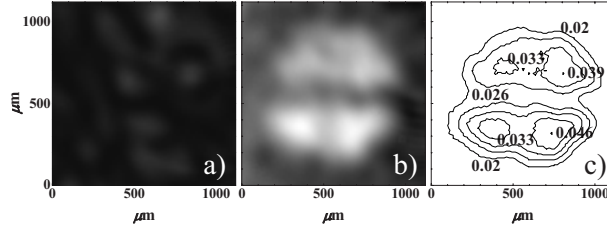


Fig. 2. a) A typical chaotic single-shot Map recorded in the Reference arm; b) Ghost image of the object obtained by evaluating $C(\mathbf{x}_R)$ over 9500 laser shots; c) contour plot of the local visibility, $\mathcal{V}(\mathbf{x}_R)$, for $N = 9500$.

The experimental results are shown in Fig. 2: panel a) displays a typical sample of chaotic intensity map $\mathcal{I}_R(\mathbf{x}_R)$ recorded in single shot, whereas panel b) contains the map of the correlation coefficients

$$C(\mathbf{x}_R) = \frac{G^{(2)}(\mathbf{x}_R)}{\sqrt{\sigma^2(I_R(\mathbf{x}_R))\sigma^2(I_T)}} \quad (9)$$

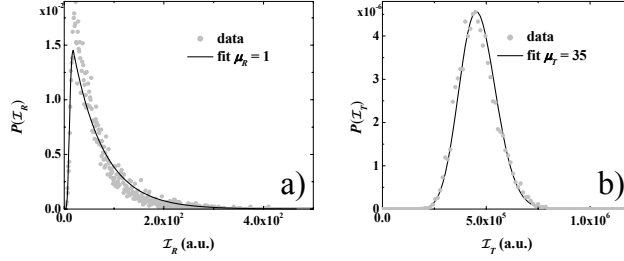


Fig. 3. a) Statistical distribution of the intensity in a single pixel of the D_R detector (dots) and multithermal fit giving $\mu_R = 1$ (full line); b) statistical distribution of the intensity on the bucket detector (dots) and multithermal fit giving $\mu_T = 35$ (full line).

evaluated over an ensemble of 9500 single shot Maps, where $\sigma^2(I) = \langle I^2 \rangle - \langle I \rangle^2$ and both intensities and variances were evaluated by subtracting the statistical contributions of the background noise. To measure the noise we considered the values recorded by the CCD in a non-illuminated sensor region. Panel b) in Fig. 2 shows that the recovered image has the correct size, as compared to the original object, being $M = 0.5$.

To quantify the quality of our technique, we define the local visibility of the reconstructed image at each point \mathbf{x}_R (see Ref.¹³) as

$$\mathcal{V}(\mathbf{x}_R) = \frac{G^{(2)}(\mathbf{x}_R)}{\langle I_R(\mathbf{x}_R)I_T \rangle} = \frac{G^{(2)}(\mathbf{x}_R)}{\langle I_R(\mathbf{x}_R) \rangle \langle I_T \rangle + G^{(2)}(\mathbf{x}_R)} \quad (10)$$

and evaluate it for the ghost image in Fig. 2 b). In Fig. 2 c) we show the contour plot of $\mathcal{V}(\mathbf{x}_R)$ at the marked levels including the maximum value 0.046.

It has been reported¹³ that there is a tradeoff between visibility and resolution of the reconstructed image that depends on the number of spatial modes (coherence areas, A_{coh}) that illuminate an object of area A_{obj} . In our case $A_{obj}/A_{coh} \simeq 1600^2/320^2 = 25$. Being this number rather low, we observe a quite poor image resolution and a quite high visibility. To confirm our results we calculate the number of modes, both spatial and temporal, involved in the interaction. We start by studying the statistical distributions of the beam intensities detected either in a single pixel \mathbf{x}_R or by the bucket detector in the Test arm. In Fig. 3 we show the experimental distributions along with the best fitting curves obtained by convolving the theoretical multithermal distribution^{14,15}

$$P_\mu(\mathcal{I}) = \frac{e^{-\mu\mathcal{I}/\langle I \rangle} \mathcal{I}^{\mu-1}}{(\langle I \rangle/\mu)^\mu (\mu-1)!} \quad (11)$$

with the experimental one obtained for the background. Here \mathcal{I} indicates the single-shot

values of either $\mathcal{I}_R(\mathbf{x}_R)$ or \mathcal{I}_T , whose mean values and variances obviously coincide with those of the operators $I_R(\mathbf{x}_R)$ and I_T . From the data in panel a) we obtained $\mu_R = 1$, independently of the position \mathbf{x}_R we tested, and $\mu_T = 35$ from the data in panel b). As the statistical distribution in Fig. 3 a) reflects the behavior of the field from shot to shot, we interpret μ_R as the number of temporal modes in the field.^{14,15} On the other hand, we can interpret μ_T as the product of the number of temporal modes times that of the spatial modes in the area covered by the 110×110 pixels of D_T . As $\mu_R \simeq 1$ we conclude that we have a number of spatial modes in the bucket, 35, greater than the number, 25, of those illuminating the object (see above): this is to be expected as the bucket integration extended on an area wider than A_{obj} . From Eq. (11) we get $\sigma^2(I_{R,T}) = \langle I_{R,T} \rangle^2 / \mu_{R,T}$, which allows linking the visibility of Eq. (10) to the number of thermal modes in the incoherent Test and Reference beams. By using Eq. (9) we can rewrite Eq. (10) as

$$\begin{aligned} \mathcal{V}(\mathbf{x}_R) &= \frac{C(\mathbf{x}_R)}{\langle I_R(\mathbf{x}_R) \rangle \langle I_T \rangle / \sqrt{\sigma^2(I_R(\mathbf{x}_R)) \sigma^2(I_T)} + C(\mathbf{x}_R)} \\ &= \frac{C(\mathbf{x}_R)}{\sqrt{\mu_R \mu_T} + C(\mathbf{x}_R)}, \end{aligned} \quad (12)$$

and make an independent estimation of $\sqrt{\mu_R \mu_T}$ as a function of the experimental values of correlation coefficients and visibility. By this method we find $\sqrt{\mu_R \mu_T} \simeq 6.8$. We consider the fact that, from the fits in Fig. 3, we found the value $\simeq 5.9$ as a proof that all the experimental results are self-consistent.

In conclusion, we have implemented a new source of correlated beams that is suitable to perform ghost imaging experiments and, as we expect, ghost diffraction too. The major benefit of this source as compared to those operating on spontaneous PDC is the possibility of tuning resolution and visibility of the ghost image, for instance by modifying the spatial coherence properties of the seed beam. In fact we observed that the coherence structure of the seed is preserved on both arms of the seeded PDC emission. Moreover, our source displays interesting features typical of spontaneous PDC with the advantage that the detectors measure intense light.

The Authors thank Matteo Paris (University of Milan) for fruitful discussions.

References

1. T. B. Pittman, Y. H. Shih, D. V. Strekalov, and A. V. Sergienko, Phys. Rev. A **52**, R3429 (1995).
2. A. Valencia, G. Scarcelli, M. D'Angelo, and Y. H. Shih, Phys. Rev. Lett. **94**, 063601 (2005).
3. D. Zhang, Y. H. Zhai, L. A. Wu, and X. H. Chen, Opt. Lett. **30** 2354 (2005).

4. F. Ferri, D. Magatti, A. Gatti, M. Bache, E. Brambilla, and L. A. Lugiato, Phys. Rev. Lett. **94**, 183602 (2005).
5. M. D'Angelo and Y. H. Shih, Laser Phys. Lett. **2**, 567 (2005) and references therein.
6. F. T. Arecchi, Phys. Rev. Lett. **15**, 912 (1965).
7. E. Brambilla, A. Gatti, M. Bache, and L. A. Lugiato, Phys. Rev. A **69**, 023802 (2004).
8. Manuscript in preparation.
9. A. Peres, Phys. Rev. Lett. **77**, 1413 (1996).
10. P. Horodecki, Phys. Lett. A **232**, 333 (1997).
11. R. Simon, Phys. Rev. Lett. **84**, 2726 (2000).
12. J. W. Goodman, *Fourier Optics* (McGraw-Hill, New York, 1968).
13. A. Gatti, M. Bache, D. Magatti, E. Brambilla, F. Ferri, and L. A. Lugiato, J. Mod. Opt. **53**, 729 (2006).
14. F. Paleari, A. Andreoni, G. Zambra, and M. Bondani, Opt. Express **12**, 2816 (2004).
15. L. Mandel and E. Wolf, *Optical Coherence and Quantum Optics* (Cambridge U. Press, Cambridge, 1995).